

## Aerodynamic performance of a novel wind barrier for train-bridge system

Xuhui He<sup>1,2a</sup>, Kang Shi<sup>1,2b</sup>, Teng Wu<sup>\*3</sup>, Yunfeng Zou<sup>1,2c</sup>,  
Hanfeng Wang<sup>1,2d</sup> and Hongxi Qin<sup>1,2e</sup>

<sup>1</sup>School of Civil Engineering, Central South University, Changsha, 410075, China

<sup>2</sup>National Engineering Laboratory for High Speed Railway Construction, Changsha, 410075, China

<sup>3</sup>Department of Civil, Structural and Environmental Engineering,  
University at Buffalo-The State Univ. of New York, Buffalo, NY 14260, USA

(Received March 30, 2016, Revised June 15, 2016, Accepted June 17, 2016)

**Abstract.** An adjustable, louver-type wind barrier was introduced in this study for improving the running safety and ride comfort of train on the bridge under the undesirable wind environment. The aerodynamic characteristics of both train and bridge due to this novel wind barrier was systematically investigated based on the wind tunnel tests. It is suggested that rotation angles of the adjustable blade of the louver-type wind barrier should be controlled within  $90^\circ$  to achieve an effective solution in terms of the overall aerodynamic performance of the train. Compared to the traditional grid-type wind barrier, the louver-type wind barrier generally presents better aerodynamic performance. Specifically, the larger decrease of the lift force and overturn moment of the train and the smaller increase of the drag force and torsional moment of the bridge resulting from the louver-type wind barrier were highlighted. Finally, the computational fluid dynamics (CFD) technique was applied to explore the underlying mechanism of aerodynamic control using the proposed wind barrier.

**Keywords:** louver-type wind barrier; aerodynamic coefficients; wind tunnel test; CFD

### 1. Introduction

Wind-induced effects on the high-speed railway is a critical issue that plays a significant role in running safety and ride comfort of the trains (Charuvisit *et al.* 2004, Dorigatti *et al.* 2012, Cai *et al.* 2015). Railway bridges are widely used for high-speed lines (e.g., over 80% of the total length of the Beijing-Shanghai high-speed railway line in China consists of bridges), hence, the aerodynamics of the train-bridge system attracts great attention (Raghunathan *et al.* 2002, Kwon *et al.* 2011, Kim *et al.* 2011, Kozmar *et al.* 2012, Han *et al.* 2015). Currently, there are mainly two

---

\*Corresponding author, Assistant Professor, E-mail: [tengwu@buffalo.edu](mailto:tengwu@buffalo.edu)

<sup>a</sup> Professor, E-mail: [xuhuihe@csu.edu.cn](mailto:xuhuihe@csu.edu.cn)

<sup>b</sup> Ph.D., E-mail: [shikang@csu.edu.cn](mailto:shikang@csu.edu.cn)

<sup>c</sup> Lecturer, E-mail: [yunfengzou@csu.edu.cn](mailto:yunfengzou@csu.edu.cn)

<sup>d</sup> Professor, E-mail: [wanghf@csu.edu.cn](mailto:wanghf@csu.edu.cn)

<sup>e</sup> Ph.D., E-mail: [qinhongxi@csu.edu.cn](mailto:qinhongxi@csu.edu.cn)

ways to handle wind-induced undesirable effects on the running safety of trains (Imai *et al.* 2012). One is based on the traffic control such as limiting speed or suspending service (He *et al.* 2014); the other is to utilize reliable engineering measures including wind barrier and aerodynamic shape optimization of the train (Suzuki *et al.* 2003, Cheli *et al.* 2010, Zhang *et al.* 2015, Xiang *et al.* 2015). The former approach is actually quite expensive, while the latter method, although presents great promise as applied to Japan's Shinkansen (Fujii *et al.* 1999, Noguchi *et al.* 2000) and China's Lanzhou-Urumqi high-speed railway (Guo *et al.* 2015), needs further investigation.

Actually, a large number of researchers have investigated the aerodynamics improvement of the train-bridge system due to wind barriers using the wind tunnel tests (e.g., Kozmar *et al.* 2014, Ogueta-Gutierrez *et al.* 2014, He *et al.* 2014) or computational fluid dynamics (CFD) (e.g., Chu *et al.* 2013, Zhao *et al.* 2015), which resulted in a number of valuable findings. For example, Zhang *et al.* (2013) studied the dynamic response of bridge and the running safety index of train with and without wind barriers under cross winds. Chu *et al.* (2013) explored that the protective effects of porous windbreak on road vehicle under crosswind using wind tunnel experiments and CFD with a large eddy simulation (LES) model. Kozmar *et al.* (2014) studied the wind barrier mechanism in combination with wind tunnel tests and particle image velocimetry (PIV) technology. Ogueta-Gutierrez *et al.* (2014) investigated the effects of curve and straight wind barriers on the bridge aerodynamic coefficients. He *et al.* (2014) examined the effects of train aerodynamic coefficients in various heights and ventilation ratios using the pressure tests, and discussed the obtained results from fluid mechanics aspects. Guo *et al.* (2015) analyzed the effects of wind barriers on the running safety of a high-speed train subjected to cross winds when it passes over the box-beam and trough-beam bridges. The abovementioned studies, however, were concentrated on traditional grid-type wind barriers at various heights, ventilation ratios and train-bridge combinations. Since the ventilation ratio of the traditional wind barriers is typically changeless after installed on the bridge, it is not convenient to apply in regions with complex wind environments. In this study, the aerodynamic performance of an adjustable, louver-type wind barrier for the train-bridge system will be discussed.

## 2. Louver-type wind barrier

The novel wind barrier was inspired by the mechanism of louver principle, hence, it is referred as to the "louver-type wind barrier" where the porosity factor and flow direction could be modified by the rotation of wind blades. The work principle of louver-type wind barrier is shown in Fig. 1. Assume that  $0^\circ$  be the initial state, the blade rotation angle could vary from  $0^\circ$  to  $180^\circ$ . When the blade is at the initial state, the porosity factor is 0%. The blade is defined as upward inclined when the rotation angle is from  $0^\circ$  to  $90^\circ$ , while downward inclined from  $90^\circ$  to  $180^\circ$ . The porosity factor is to be maximized at  $90^\circ$ , and the blade returns back to the initial state at  $180^\circ$ . Compared with the traditional wind barrier, the novel wind barrier can be adjusted according to various incident wind speeds and directions.

The wind barrier porosity factor  $\beta$  is defined as

$$\beta = \frac{A_v}{A_r} \quad (1)$$

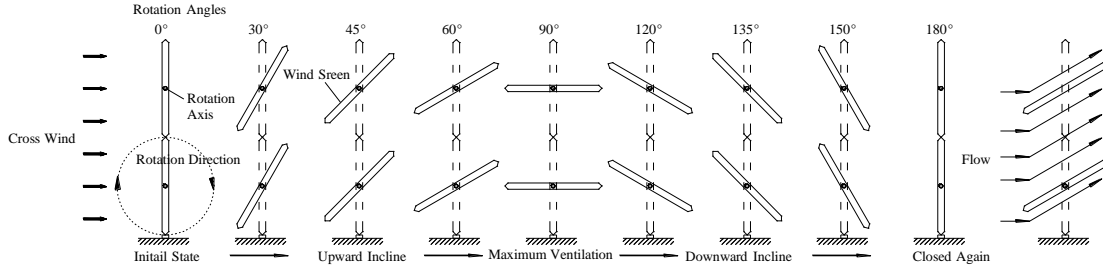


Fig. 1 Work principle of louver-type wind barrier

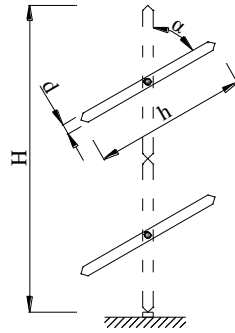


Fig. 2 Key parameters of the louver-type wind barrier

where  $A_v$  is the gap area of the wind barrier and  $A_T$  total area expressed as

$$A_v = \begin{cases} hL(1 - \cos\alpha)n & (\alpha \neq 90^\circ) \\ (h - d)Ln & (\alpha = 90^\circ) \end{cases} \quad (2)$$

$$A_T = hLn \quad (3)$$

where  $h$  and  $d$  are the width and thickness of a blade, respectively;  $L$  is the length of wind barrier;  $n$  is the number of blade layers;  $\alpha$  is the rotation angle with values ranging from  $0^\circ$  to  $180^\circ$  in clockwise. Some key parameters of the louver-type wind barrier are illustrated in Fig. 2.

The aerodynamic coefficients of train and bridge in the body-axis system are defined in Fig. 3 and expressed as

$$C_D^i = \frac{2F_x^i}{\rho U^2 H^i} \quad (4)$$

$$C_L^i = \frac{2F_y^i}{\rho U^2 B^i} \quad (5)$$

$$C_M^i = \frac{2M^i}{\rho U^2 (B^i)^2} \quad (6)$$

where  $F_x^i$ ,  $F_y^i$  and  $M^i$  ( $i=b$  or  $t$ , representing bridge or train, respectively) are the drag force, lift force and overturning moment of bridge or train model;  $C_D^i$ ,  $C_L^i$  and  $C_M^i$  ( $i=b$  or  $t$ ) are corresponding the drag force, lift force and overturning moment coefficients;  $\rho$  is the air density ( $\rho=1.225 \text{ kg/m}^3$ );  $U$  is the reference velocity;  $H^i$  and  $B^i$  ( $i=b$  or  $t$ ) are the characteristics of height and width of bridge or train model, respectively. The center of leeward track is chosen as moment origin of train, while the model centroid is selected as moment origin of bridge.

### 3. Wind tunnel tests

#### 3.1 Test models

The train-bridge system under investigation is based on a specific rail-transit bridge located in Chongqing, China. The bridge is a twin tower hybrid cable-stayed bridge with double cable planes. The main span is 340 m, with a width of 19.6m and a beam height of 3.0 m. Considering several factors such as the blockage ratio and Reynolds number effects, the scale ratio was chosen to be 1:40 for all test models. The length, height, and width of the bridge model are 2000 mm, 490 mm and 73 mm, respectively, while the train model are 2000 mm, 89 mm, and 109 mm, respectively.

Sketch of the tested train and bridge models together with their detailed size are shown in Fig. 4. The maximum blockage ratio is 4.2% which generates insignificant effects on test results (Holmes 2007).

While the geometric similarity is strictly satisfied, some associated details of the bridge deck and train are ignored in the tests. The models of both train and bridge girder are made of rolled steel to obtain adequate strength and stiffness during the experiments and measurements.

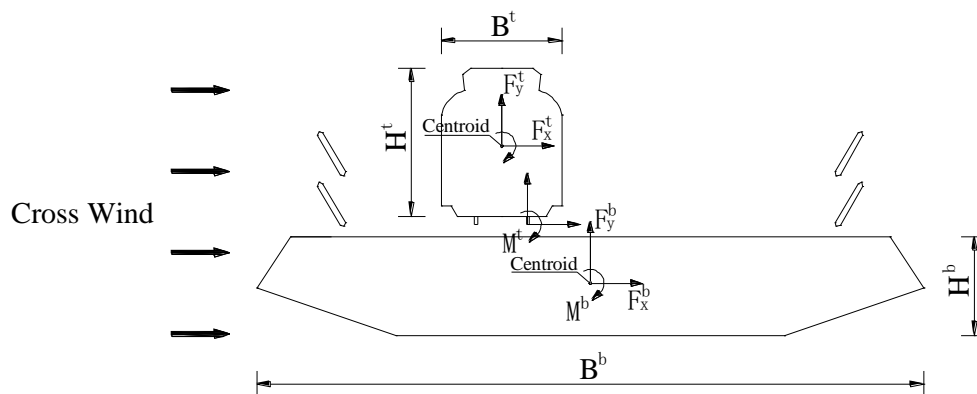


Fig. 3 Aerodynamic force in body-axis coordinate

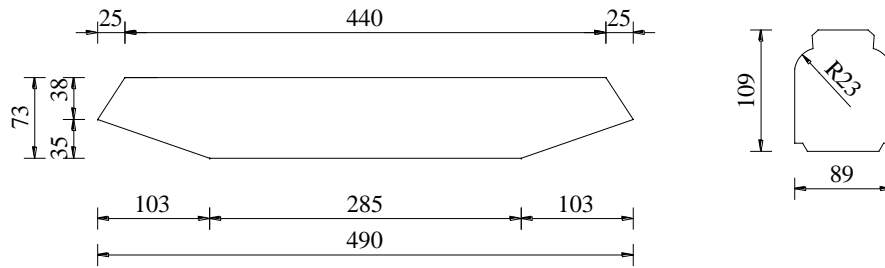


Fig. 4 Geometric dimension of the models (unit: mm)

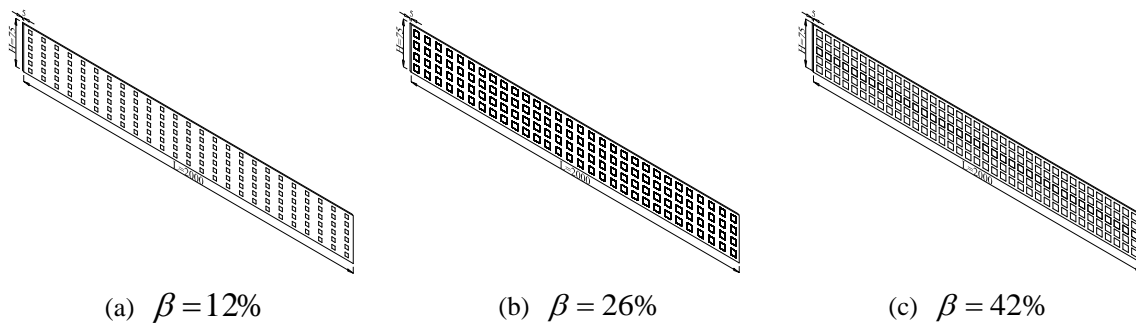


Fig. 5 Model dimensions of grid-type wind barriers (unit: mm)

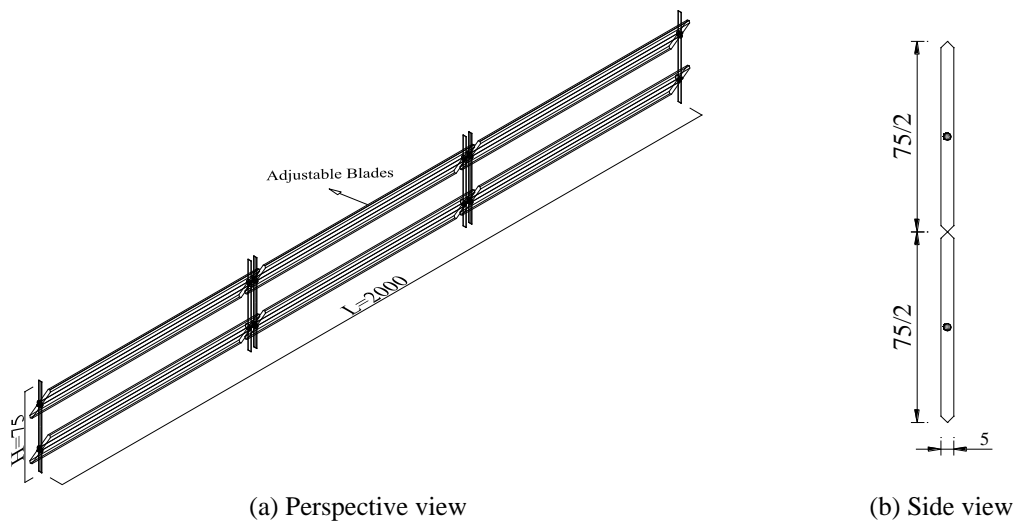


Fig. 6 Model dimensions of louver-type wind barriers (unit: mm)

The height ( $H$ ), length ( $L$ ) and thickness ( $d$ ) of the louver-type wind barrier are 75 mm, 2000 mm and 5 mm (corresponding to a prototype height of 3m). Specifically, the two-layer wind barrier is analyzed in this study, i.e.,  $n=2$ . Three different porosity factors of 12%, 26% and 42% are accounted for to design the grid-type wind barriers, which corresponds to rotation angles of louver-type wind barrier at  $30^\circ$ ,  $45^\circ$  and  $60^\circ$ , respectively. Xiang *et al.* (2013) demonstrated that the various opening forms of wind barrier have similar effects on train aerodynamics and that the appropriate aperture size is 8 mm-12 mm. Accordingly, the type of square hole array was used for grid-type wind barriers in this study. The geometric dimensions of louver-type and traditional grid-type wind barriers are shown in Figs. 5 and 6.

### 3.2 Measurement system

In order to synchronously measure the individual aerodynamic forces of the train and of the bridge, a set of train-bridge separation measurement system was developed, as presented in Fig. 7. Train and bridge models are fixed on a rotatable disc, and there is a small gap between train and bridge to obtain individual aerodynamic forces. The train model can move horizontally along the slider, while the slider can move up and down along the curved chute. As a result, the relative position of train and bridge can be adjusted. Both train and bridge models are equipped with high-frequency force balance at each end, which are IFS-type six-component dynamic balance (with a force resolution of 0.02 N) produced by NITTA company of Japan. For each measurement, the sampling duration was selected to be 30s with a sampling frequency of 1 kHz. A special data acquisition software was used in this study to synchronously record the data of four balances. Disc, train model and bridge model can coaxially rotate around the balance at the end of bridge model to adjust the wind attack angle. A series of location holes were designed on the disc to ensure the accuracy of the wind attack angle adjustment.

The test was conducted in the high-speed test segment of wind tunnel in the Central South University. The dimension of the high-speed test segment is  $15\text{ m}\times 3\text{ m}\times 3\text{ m}$  (length, width and height, respectively). Schematic diagram of the wind tunnel is shown in Fig. 8. The continuously adjustable wind speed ranges from 5 m/s to 94 m/s. All tests were conducted in a uniform oncoming flow with wind velocity  $U=10\text{ m/s}$ , and the corresponding Reynolds number of train-bridge system is  $1.61\times 10^5$ . The turbulence intensity  $I_u$  was controlled within 0.5%.

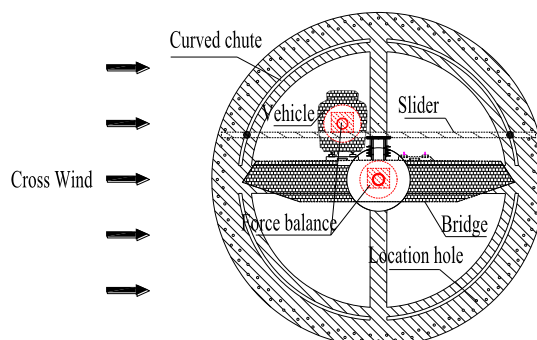


Fig. 7 Schematic diagram of train-bridge separation measurement system

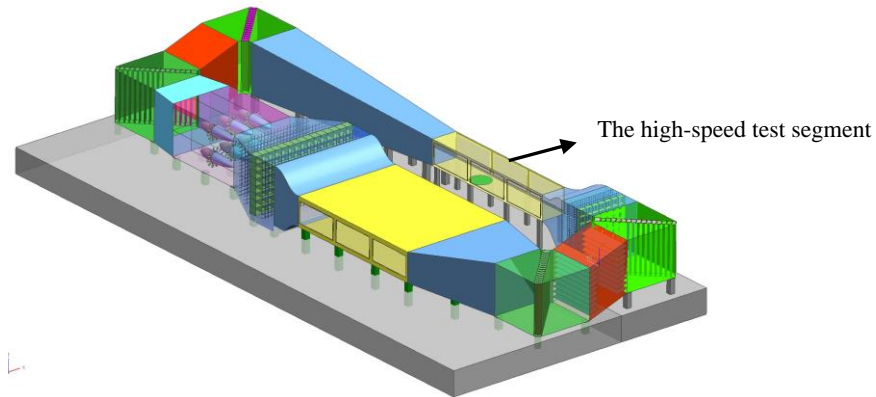
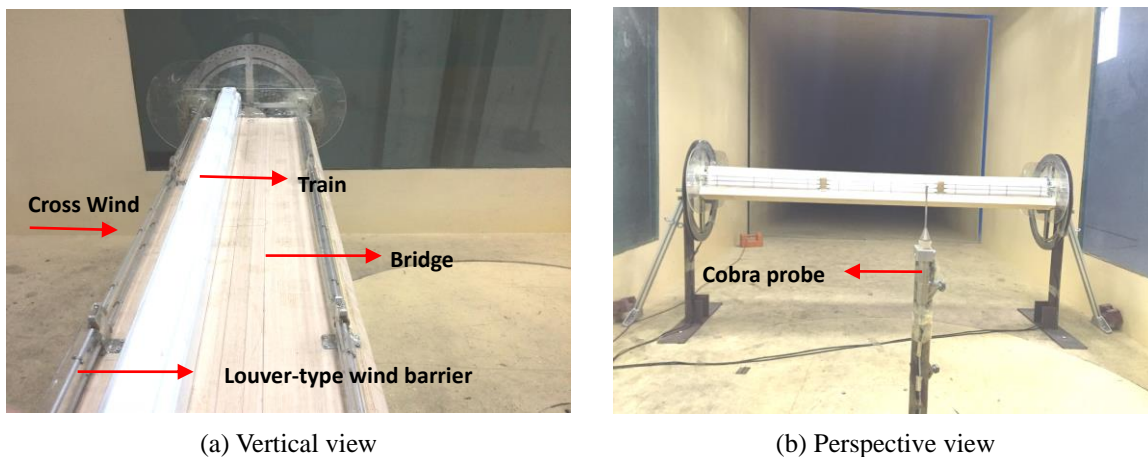


Fig. 8 Schematic diagram of the wind tunnel



(a) Vertical view

(b) Perspective view

Fig. 9 Wind measurement system in the wind tunnel

Although Reynolds number may affect the aerodynamic coefficients of train-bridge system, for the purpose of investigating aerodynamic performance of the novel wind barrier, it is believed that Reynolds number has similar effects on various cases in this study. Hence, Reynolds number effects on the aerodynamic coefficients of the train-bridge system will not be discussed here (Chen *et al.* 2015). The flow velocity was recorded using an Australian TFI cobra probe located at the centerline of the test section (1.5 m upstream the tested model and the same height with top surface of the bridge model), as indicated in Fig. 9.

## 4. Experimental results and discussion

### 4.1 Validation of the measurement system

Two approaches namely separated and unified train-bridge systems were utilized to validate the reliability of train-bridge separation measurement system. In the unified train-bridge test, train was fixed on the windward or leeward side, and the gap between train and bridge was same with the separated test. The test results are listed in Table 1. From the table it can be concluded that the result errors for both windward and leeward cases are less than 5%, which manifested high fidelity of the separation measurement system in this study.

#### 4.2 Comparison of louver-type and grid-type wind barriers

The compared results between louver-type and grid-type wind barriers are shown in Fig. 10. The tested results of no wind barrier are also given in the figures. It should be noted that the blade thickness is considered in the comparison of these two types of wind barriers. As can be seen from the figures, compared to the aerodynamic performance of grid-type wind barriers, although louver-type wind barrier may slightly increase the lift coefficient of the bridge and drag coefficient of the train, it would significantly reduce the moment coefficients for both bridge and train. Among various porosity factors, the maximum decreases are 51% and 23% for the bridge and the train, respectively. Therefore, louver-type wind barriers may be a better option for train traffic safety compared to grid-type wind barriers from the aerodynamic view point. It can also be seen that the three aerodynamic coefficients of train for both louver-type and grid-type wind barriers are less than the results without any, but opposite situation is observed for the bridge drag and moment coefficients. Generally, the wind barriers are beneficial to the train, while slightly negative effects may be generated on the bridge. Thus, it is necessary to consider the negative impact when the wind barrier are installed on the bridge. It is important to note that moment coefficients for both bridge and train increase with the selected three porosity factors (i.e., 12%, 26% and 42%), corresponding to rotation angles of 30°, 45° and 60°, respectively. Actually, moment coefficients of bridge and train are monotonic increasing functions with respect to the rotation angles within the range of 0° to 90°.

#### 4.3 The effects of rotation angle

The rotation angles of 0°, 30°, 45°, 60°, 90°, 120°, 135° and 150° (with symmetric rotation as indicated in Table 2) were employed to investigate the aerodynamics of train and bridge at various rotation angles. Tested train was located in the windward side, and other specific conditions are listed in Table 2.

Table 1 Validity test results for the measurement system

Test cases	Tested train located on the windward side			Tested train located on the leeward side		
	$C_D$	$C_L$	$C_M$	$C_D$	$C_L$	$C_M$
Train+Bridge(Separated test)	1.368	-0.648	0.263	1.434	-0.744	0.313
Train+Bridge(Unified test)	1.395	-0.625	0.274	1.467	-0.723	0.327
Error	2.0%	3.5%	4.2%	2.3%	2.8%	4.5%

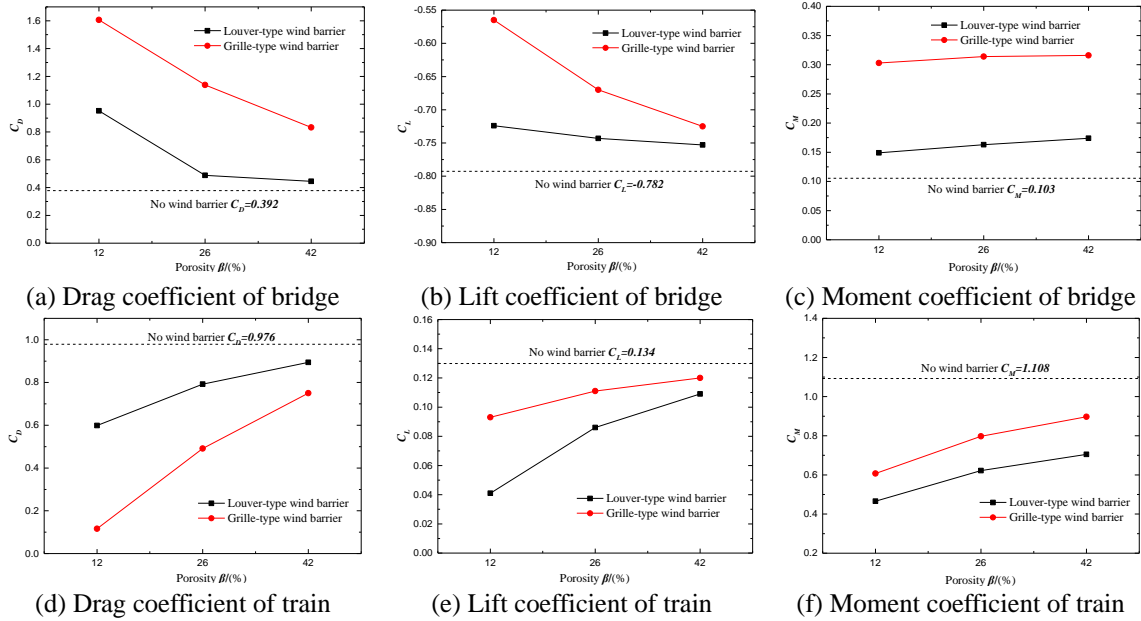


Fig. 10 Comparison of aerodynamic coefficients of bridge and train between louver-type and grid-type wind barriers

Table 2 Cases of various rotation angles

Rotation angle $\alpha$ (°)	Relative position diagram between bridge and train	Blade layer numbers	Rotation form	Layout form
0, 30, 45, 60, 90, 120, 135, 150		Two layers	Symmetry rotation	Double layout

The test results are shown in Fig. 11. The figure indicates that rotation angles present significant effects on drag coefficients of both bridge and train. Drag coefficient of bridge first decreases and then increases, and reaches the minimum value at 90° (with maximum porosity factor). Opposite situation is observed for the drag coefficient of train.

As for the lift coefficient of bridge, an increase (a negative sign represents that the lift direction is downward) appears from 0° to 30°. The increasing tendency of the lift coefficient is not obvious within 30°-90°, and it slightly decreases when the rotation angle exceeds 90°. There is a large difference between train and bridge for the change trend of lift coefficient. The lift coefficient of train monotonically increases within 30°-120° and the maximum value is at 120°. Despite the decrease of the porosity factor when the rotation angle increases from 90° to 120°, the air flow is redirected to attack to the base (or lower part) of the train. The combination effects of the aforementioned two aspects result in a increase of the lift coefficient until 120°. Beyond this, the

lift coefficient of train decreases but the value is still larger than those of the rotation angles in 0°-90°.

The value of the moment coefficient of bridge fluctuates around 0.1 in 0°-150°. While the moment coefficient of bridge is insignificantly affected by rotation angles, the moment coefficient of train is obviously affected by rotation angles and the trend is shown to first increase and then decrease with a maximum at 90°. It is suggested that the rotation angle should be controlled within 90° considering the safety running of trains based on the results presented in Fig. 11.

It should be noted that the aerodynamic coefficients for both bridge and train at 90° indicated in the dashed rectangular frame (Fig. 11) are different with no wind barrier values. The reason is that the porosity factor of wind barrier at the rotation angle of 90° is different from the case of no wind barrier ( $\beta=100\%$ ). The porosity factor of wind barrier at 90° is 87% in this study ( $d=5\text{ mm}$ ).

#### 4.4 The effects of rotation form

If louver-type wind barriers are installed on both sides of bridge, it is necessary to consider the effect of rotation forms for the aerodynamic characteristics of bridge-train system. Therefore, this study also examined the aerodynamic performance of both symmetric and anti-symmetric rotation forms. The tested train was located on the windward side. The specific conditions are shown in Table 3.

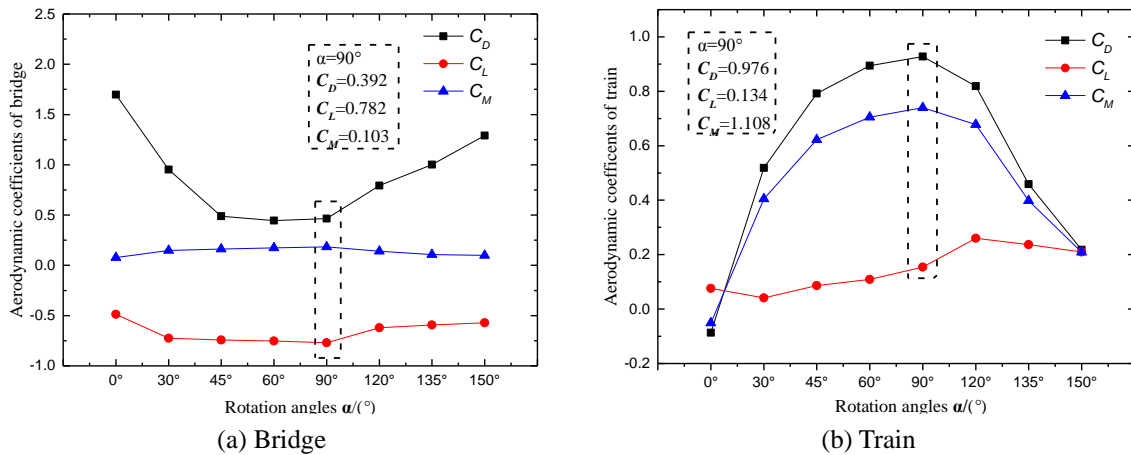


Fig. 11 Aerodynamic coefficients of bridge and train in various rotation angles

Table 3 Cases of two different rotation forms

Rotation forms	Symmetric	Anti-symmetric
Case representation		

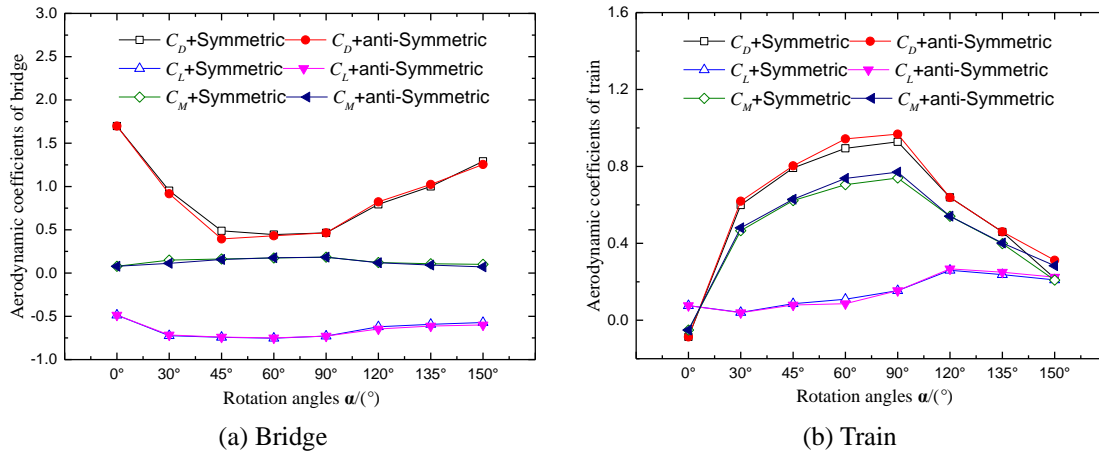


Fig. 12 Aerodynamic coefficients of bridge and train in two different rotation forms

Fig. 12 illustrates the tested results from two different rotation forms, which present insignificant influence on the aerodynamic coefficients of bridge and train. Compared with lift and moment coefficients, drag coefficient is more sensitive to blade rotation forms. For bridge drag coefficient, the value of symmetric rotation is greater than the anti-symmetric rotation for blade angles smaller than  $90^\circ$ . However, the results are opposite when blade angles are greater than  $90^\circ$ . For the drag coefficient of train, the value of anti-symmetric rotation is always greater than that of the symmetric case. Thus, the symmetric rotation form seems more beneficial to the aerodynamics of the train-bridge system. It should be noted that only windward case is studied here. For the leeward case, it is expected that the tested results of symmetric and anti-symmetric situations will present larger discrepancy due to the wake effects.

#### 4.5 The effects of train-bridge combination type

The train may be located in the windward, leeward or both under cross wind action, hence, three different train-bridge combination types were selected for wind tunnel tests, as indicated in Table 4. It should be noted that only the symmetric rotation form was utilized in the study. He *et al.* (2014) demonstrated that the wind barrier has less impact on the aerodynamic forces of the leeward train due to the blocking effects from windward train. Therefore, only aerodynamic force of the windward train was measured for the case of two-trains.

Table 4 Cases of various train-bridge combination types

Train-bridge combined types	Two trains + Bridge	Windward + Bridge	Leeward + Bridge
Case representation			

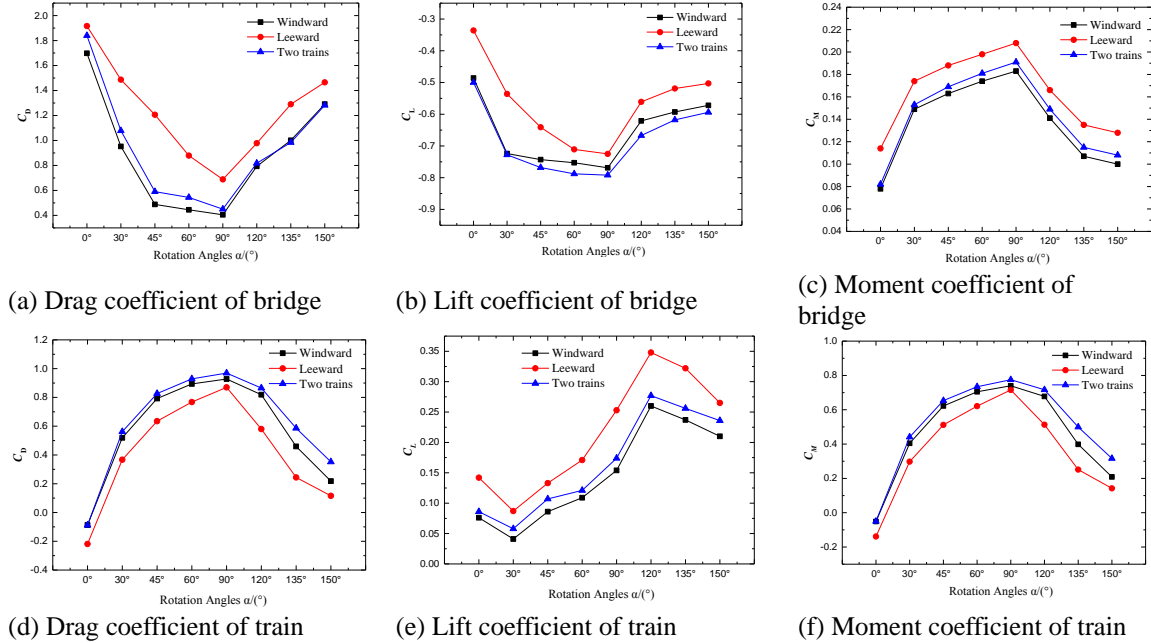


Fig. 13 Aerodynamic coefficients of bridge and train in various train-bridge combination types

The test results are shown in Fig. 13. The trends of aerodynamic coefficients of bridge and train with rotation angles in different train-bridge combination types are basically similar, but their values are greatly influenced by the train location. The aerodynamic coefficients present large fluctuations, especially as the train is located in the leeward side. According to Figs. 13(a)-13(c), the drag and moment coefficients of bridge are significantly greater than other cases when the train is arranged on the leeward side, while the lift coefficients is relatively smaller. In terms of aerodynamic coefficients of train, both drag and moment coefficients for “Two trains + Bridge” and “Windward + Bridge” cases are larger than the tested values of “Leeward + Bridge” case, but the lift coefficient is opposite. The main reason is that the pressure on the surface of train decreases when it is located on the leeward side (more detailed discussion referred to Sect. 5). Moreover, the difference of the aerodynamic coefficients of bridge and train between “Two trains + Bridge” and “Windward + Bridge” cases is insignificant, which demonstrates the low importance of the aerodynamic influence of the leeward train in the case of “Two trains + Bridge”. The test results are consistent with the conclusions obtained in He *et al.* (2014). As a result, it is safer for trains to use the leeward side.

## 5. CFD simulations

### 5.1 Computational approach

To explore the underlying mechanism of aerodynamic control using the proposed wind barriers,

CFD technique was employed to study the change of aerodynamics of the train-bridge system under various rotation angles. The selected two-dimensional (2D) computational domain is the same with actual wind tunnel size of 15 m×3 m (length and height, respectively). The inlet boundary is the uniform flow with wind speed of 10m/s, and the velocity at the outlet boundary satisfies the zero-gradient condition. No-slip condition is applied to the upper and lower boundaries, and the bridge and train surfaces. The computational domain together with flow boundary conditions used in the simulations are illustrated in Fig. 14. In addition, the Neumann and Dirichlet pressure conditions are respectively employed at the inlet and outlet in this study. Turbulence intensity is selected as 0.5% in accordance with the measured value. Since the Mach number of cross wind is less than 0.3, the flow is treated as unsteady incompressible fluid. The commercial grid generator software ICEM-CFD was utilized to create the computational mesh (unstructured), as presented in Fig. 15. The grid refinement study was conducted to ensure the reliability of simulation results (Ferziger and Peric 1999). Specifically, six sets of grids where the minimum sizes are respectively 30 mm, 20 mm, 10 mm, 8 mm, 5 mm and 3 mm were employed in this study. The corresponding drag coefficients of the bridge are depicted in Fig. 16. It is noted that the drag coefficient of bridge remains relatively stable for minimum grid sizes smaller than 8 mm, hence, 8 mm was selected as the minimum size for simulations in this study. Reynolds-averaged Navier-Stokes (RANS) equations were solved together with shear stress transport (SST)  $k-\omega$  turbulence model (Menter 1994), where the semi-implicit method for pressure-linked equations (SIMPLE) algorithm was utilized for pressure and velocity coupling.

Fig. 17 gives the simulated and measured drag coefficients of train and bridge models. It is shown that the numerical simulations fit the tested results well and the errors are controlled within 5%, which demonstrates the high fidelity of the numerical results based on the employed simulation schemes (Marijo *et al.* 2014).

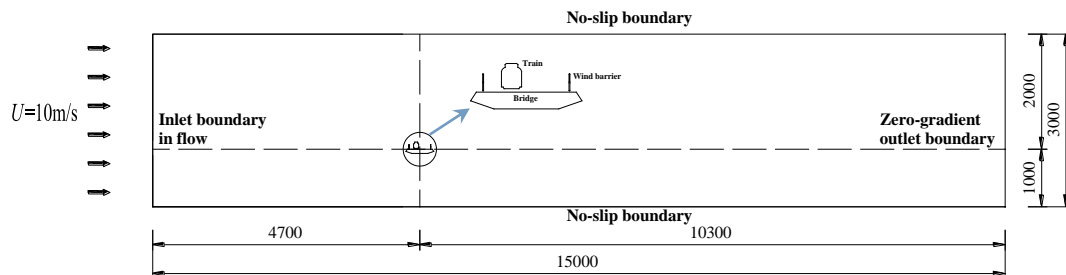


Fig. 14 Computational domain with boundary conditions (unit: mm)

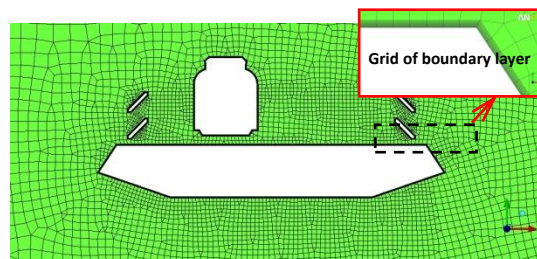


Fig. 15 Generated unstructured mesh of central part of the computational domain

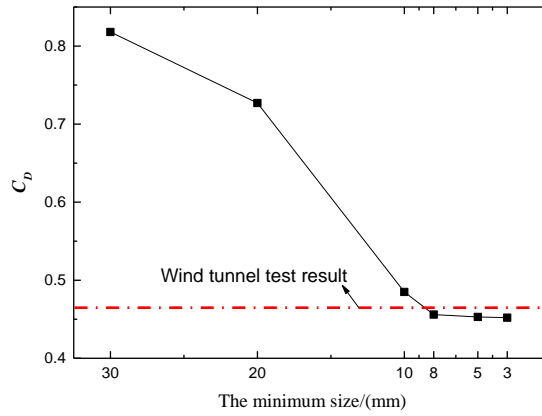


Fig. 16 Grid independence analysis

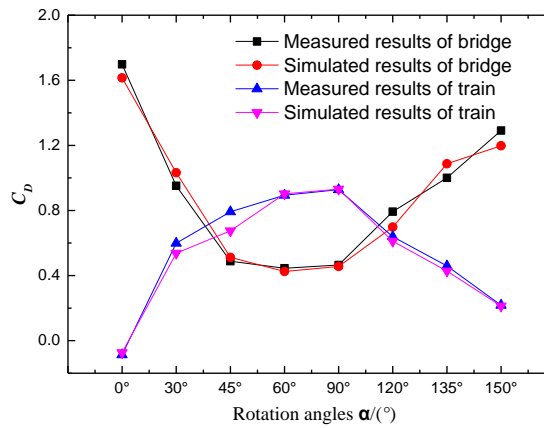


Fig. 17 Comparison of measured and simulated results

### 5.2 Effects of rotation angle

Figure 18 depicts the pressure contour around the train-bridge system with several typical rotation angles. It is shown that both windward and leeward sides of train are with negative pressure at rotation angle of  $0^\circ$ . With the increase of the rotation angle, the pressure on the windward side of train is from negative to positive and eventually the positive pressure dominates. The positive pressure domain and corresponding value reach a maximum at the rotation angle of  $90^\circ$ . As the rotation angle exceeds  $90^\circ$ , the incident flow is redirected to attack the lower part of train, and the positive pressure domain and corresponding value gradually decrease, as shown in Figs. 18(a)-18(d). Compared with windward side, the pressure on the leeward side of train remains negative and its value is less affected by the rotation angle. Since the aerodynamic drag of train is mainly obtained from the integration of pressure on the windward and leeward surfaces, it first increases and then decreases with the rotation angle and reach a maximum at  $90^\circ$ . The absolute

value of the pressure on the top of train increases with the rotation angle from  $0^\circ$  to  $90^\circ$  (e.g., from 62Pa to 80Pa), while the bottom pressure does not change significantly. Accordingly, the pressure difference between upper and lower surface increases. As the rotation angle is at  $120^\circ$ , the incident flow is redirected to attach the lower part of the train with accelerated flow velocity. As a result, the absolute value of the bottom pressure increases (e.g., from 36Pa to 23Pa), while the top pressure remains unchanged (around 80Pa). This results in a further increase of the pressure difference at the rotation angle of  $120^\circ$ . As the rotation angle exceeds  $120^\circ$ , however, the decrease of the porosity factor leads to obvious decrease of the pressure difference. Since the aerodynamic lift of train is mainly obtained from integrated of pressure on the upper and lower model surfaces, it first increases and then decreases with the rotation angle and reaches a maximum at  $120^\circ$ . Train moment coefficient is basically obtained as a product of the aerodynamic force and the lever arm where the moment center is located at the rail center point on the leeward side. Therefore, moment coefficient changes according to the variation of lift and drag coefficients.

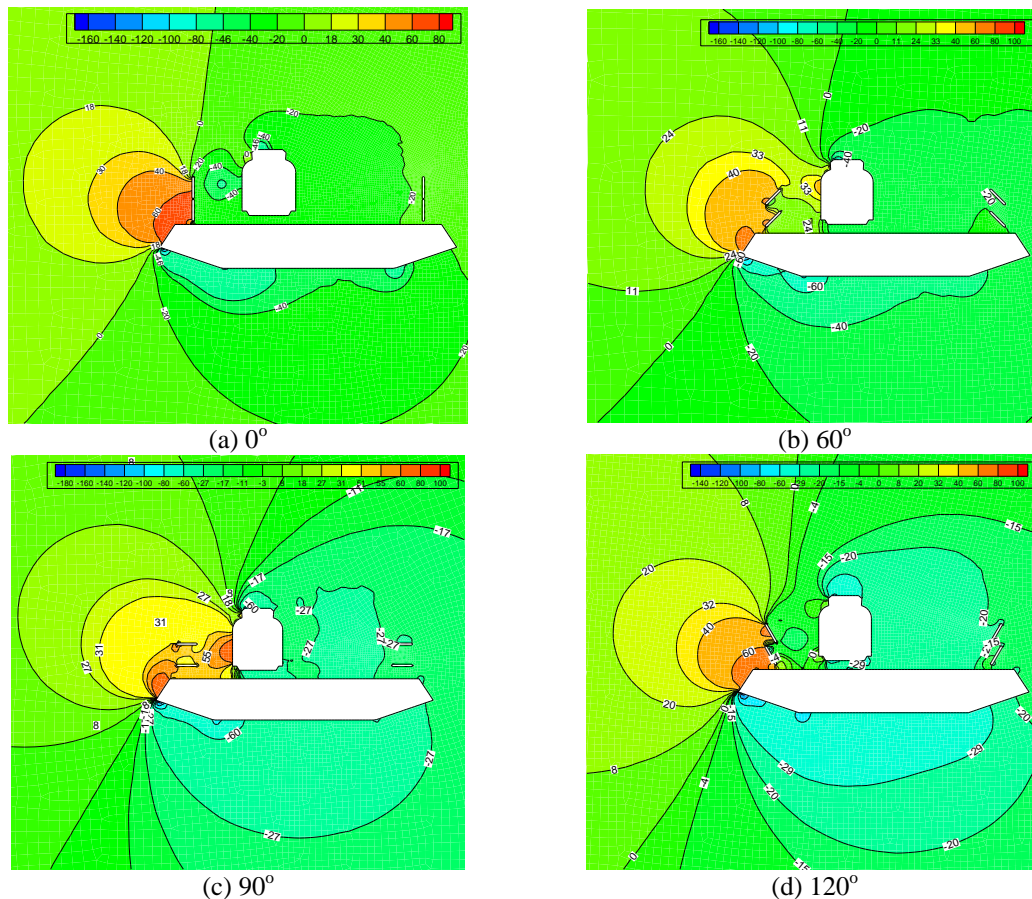


Fig. 18 Pressure contour around train-bridge system with typical rotation angles (unit: Pa)

### 5.3 Effects of rotation form and combination type

In this study, the case of  $45^\circ$  is utilized to analyze the pressure distribution with two different rotation forms, as indicated in Fig. 19. From the figure, the pressure distribution with the symmetric rotation form is similar to that in the anti-symmetric case, especially on the windward side of the train. While there is a slight difference of the pressure distribution on the leeward side of the train. Consequently, aerodynamic coefficients of the bridge and train with different rotation forms are generally consistent, which interprets the measured results in Section 4.4.

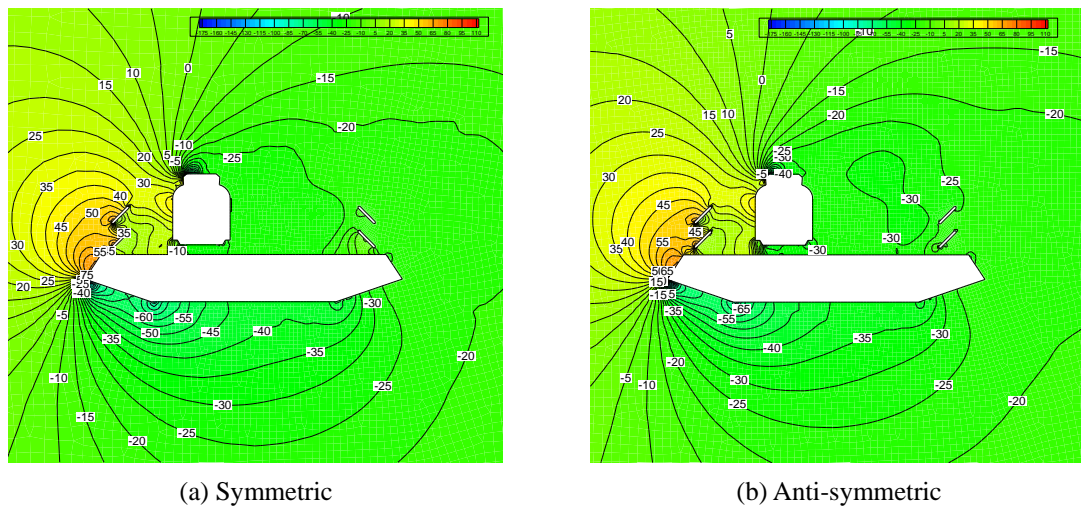


Fig. 19 Pressure contour around train-bridge system with different rotation forms (unit: Pa)

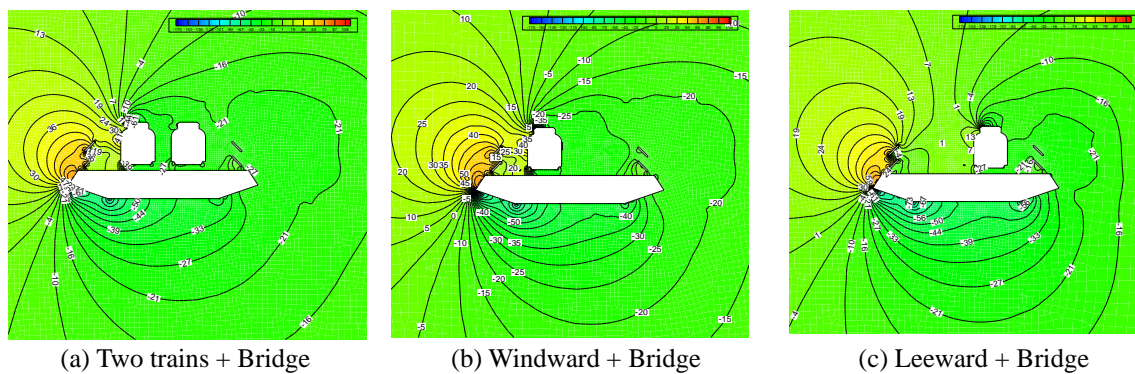


Fig. 20 Pressure contour around train-bridge system with various combination types (unit: Pa)

Fig. 20 gives the pressure contour around the train-bridge system with various combination types at  $45^\circ$ . In comparison between Figs. 20(a) and 20(b), the pressure distribution in the case of “Two trains + Bridge” is similar to that of “Windward + Bridge”, and both of them have a significant difference with the case of “Leeward + Bridge”. The covered range of positive pressure on the top of bridge for the case where the train is located in the leeward side is larger than that of the windward case, which results in a smaller lift coefficient of the bridge. The average pressure value of windward side of the train is around 13Pa in the case of “Leeward + Bridge”, which is much smaller than the value in the cases of “Two trains + Bridge” and “Windward + Bridge” (around 30Pa). This is mainly attributed to the wake decay effects since the train in the “Leeward + Bridge” case is far away from the wind barrier. Consequently, the drag and moment coefficients in the case of “Leeward + Bridge” are relatively smaller.

## 6. Conclusions

To improve the running safety of the train in the undesirable wind environment, an adjustable wind barrier was introduced in this study. The aerodynamic performance of both train and bridge due to this novel wind barrier was investigated in the wind tunnel. Furthermore, CFD technique was employed to explore the underlying mechanism of aerodynamic control using the proposed louver-type wind barrier. Although additional work based on the wind tunnel tests and CFD simulations is necessary and underway to further investigate the aerodynamic performance of the novel wind barrier with an emphasis on physical significance, some conclusions drawn from this study are:

- Compared with the aerodynamic performance of traditional grid-type wind barrier, louver-type wind barrier can greatly reduce moment coefficients for both bridge and train. Among various porosity factors investigated in this study, the maximum decreases are 51% and 23%, respectively. This indicates the louver-type wind barrier may be more beneficial to traffic safety from the aerodynamic view point.
- The rotation angle of louver-type wind barrier presents significant influence on aerodynamic coefficients of train-bridge system, especially for the drag coefficient. The drag coefficient of bridge first decreases then increases with the rotation angle, while the opposite situation is observed for the train drag coefficient. For the lift coefficient, both the bridge and train cases first increase and then decrease. The bridge lift coefficient reaches the maximum value at  $60^\circ$ , while the train lift coefficient is a monotonically increasing function with respect to the rotation angle in the range from  $30^\circ$  to  $120^\circ$ . The moment coefficient of train first increases and then decreases, however, the bridge case is not sensitive to the rotation angle. Generally, it is suggested that the rotation angle should be controlled within  $90^\circ$  in the consideration of running safety.
- Aerodynamic coefficients of train-bridge system are slightly affected by the rotation form. Specifically, the symmetrical rotation form is recommended as the louver-type wind barrier is installed on both side of bridge.
- Aerodynamic coefficients of train-bridge system are greatly influenced by various train-bridge combination types. The aerodynamic coefficients of train significantly decrease as the train is located on the leeward side. Therefore, the louver-type wind barrier presents a better aerodynamic performance for the train on the leeward side.

## Acknowledgments

Supports from the Project of Science and Technology Research and Development Program of China Railway Corporation (2015G002-C), Project of Innovation-Driven Plan in Central South University (2015CX006), the National Natural Science Foundations of China (51322808, 51508580, U1534206) and the China Postdoctoral Science Foundation Funded Project (Project No. 2014M562133) are gratefully acknowledged.

## References

- Cai, C.S., Hu, J.X., Chen, S., Han, Y., Zhang, W. and Kong, X. (2015), "A coupled wind-vehicle-bridge system and its applications: a review", *Wind Struct.*, **20**(2), 117-142.
- Charuvisit, S., Kimura, K. and Fujino, Y. (2004), "Effects of wind barrier on a vehicle passing in the wake of a bridge tower in cross wind and its response", *J. Wind Eng. Ind. Aerod.*, **92**(7), 609-639.
- Cheli, F., Corradi, R., Rocchi, D., Tomasini, G. and Maestrini, E. (2010a), "Wind tunnel tests on train scale models to investigate the effect of infrastructure scenario", *J. Wind Eng. Ind. Aerod.*, **98**, 353-362.
- Chen, N., Li, Y.L., Wang, B., Su, Y. and Xiang, H.Y. (2015), "Effects of wind barrier on the safety of vehicles driven on bridges", *J. Wind Eng. Ind. Aerod.*, **143**, 113-127.
- Chu, C.R., Chang, C.Y., Huang, C.J., Wu, T.R. and Wang, C.Y. (2013), "Windbreak protection for road vehicles against crosswind", *J. Wind Eng. Ind. Aerod.*, **116**, 61-69.
- Dorigatti, F., Sterling, M., Rocchi, D., Belloli, M., Quinn, A.D., Baker, C.J. and Ozkan, E. (2012), "Wind tunnel measurements of crosswind loads on high sided vehicles over long span bridges", *J. Wind Eng. Ind. Aerod.*, **107-108**, 214-224.
- Ferziger, J.H. and Peric, M. (1999), *Computational Methods for Fluid Dynamics*. Springer.
- Fujii, T., Maeda, T., Ishida, H., Imai, T., Tanemoto, K. and Suzuki, M. (1999), "Wind-induced accidents of train/vehicles and their measures in Japan", *Quart. Report Railway Tech. Res. Inst.*, **40**(1), 50-55.
- Guo, W.W., Xia, H., Karoumi, R., Zhang, T. and Li, X.Z. (2015), "Aerodynamic effect of wind barriers and running safety of trains on high-speed railway bridges under cross winds", *Wind Struct.*, **20**(2), 213-236.
- Han, W.S., Ma, L., Cai, C.S., Chen, S.R. and Wu, J. (2015), "Nonlinear dynamic performance of long-span cable-stayed bridge under traffic and wind", *Wind Struct.*, **20**(2), 249-274.
- He, X.H., Zou, Y.F., Wang, H.F., Han, Y. and Shi, K. (2014), "Aerodynamic characteristics of a trailing rail trains on viaduct based on still wind tunnel experiments", *J. Wind Eng. Ind. Aerod.*, **135**, 22-33.
- Holmes J.D. (2007), *Wind loading of structures*. London (UK): Taylor & Francis.
- Imai, T., Fujii, T., Tanemoto, K., Shimamura, T., Maeda, T., Ishida, H. and Hibino, Y. (2012), "New train regulation method based on wind direction and velocity of natural wind against strong winds", *J. Wind Eng. Ind. Aerod.*, **90**, 1601-1610.
- Kim D.H., Kwon, S.D., Lee, I.K. and Jo, B.W. (2011), "Design criteria of wind barriers for traffic. Part 2: decision making process", *Wind Struct.*, **14**(1), 71-80.
- Kozmar, H., Procino, L., Borsani, A. and Bartoli, G. (2012), "Sheltering efficiency of wind barriers on bridges", *J. Wind Eng. Ind. Aerod.*, **107-108**, 274-284.
- Kozmar, H., Procino, L., Borsani, A. and Bartoli, G. (2014), "Optimizing height and porosity of roadway wind barriers for viaducts and bridges", *Eng. Struct.*, **81**, 49-61.
- Kwon S.D., Kim D.H., Lee S.H. and Song H.S. (2011), "Design criteria of wind barriers for traffic. Part 1: wind barrier performance", *Wind Struct.*, **14**(1), 55-70.
- Marijo, T., Jozef, D., Franc, K. and Viktor, S. (2014), "Numerical and experimental study of the flow through a geometrically accurate porous wind barrier model", *J. Wind Eng. Ind. Aerod.*, **98**, 353-362.
- Menter, F.R. (1994), "Two-equation eddy-viscosity turbulence models for engineering application", *AIAA J.*, **32**(8), 1598-1605.

- Noguchi, T. and Fujii, T., (2000), "Minimizing the effect of natural disasters", *Jpn. Rail. Transport Rev.*, **23**, 52-59.
- Ogueta-Gutierrez, M., Franchini, S. and Alonso, G. (2014), "Effects of bird protection barriers on the aerodynamic and aeroelastic behaviour of high speed train bridges", *Eng. Struct.*, **81**, 22-34.
- Raghunathan, R.S., Kim, H.D. and Setoguchi, T. (2002), "Aerodynamics of high-speed railway train", *Pro. Aerospace Sci.*, **38**(6-7), 469-514.
- Suzuki, M., Tanemoto, K. and Maeda, T. (2003), "Aerodynamic characteristics of train/vehicles under cross winds", *J. Wind Eng. Ind. Aerod.*, **91**, 209-218.
- Xiang, H.Y., Li, Y.L. and Hu, Z. (2013), "Simulation method of porous wind screen scale model on bridge by wind tunnel tests", *Eng. Mech.*, **30**(8), 212-216. (in chinese)
- Xiang, H.Y., Li, Y.L., Wang, B. and Liao, H.L. (2015), "Numerical simulation of the protective effect of railway wind barriers under crosswinds", *Int. J. Rail Transport.*, **3**(3), 151-163.
- Zhang, T., Xia, H. and Guo, W.W. (2013), "Analysis on running safety of train on bridge with wind barriers subjected to cross wind", *Wind Struct.*, **17**(2), 203-225.
- Zhang, N., Ge, G.H., Xia, H. and Li, X.Z. (2015), "Dynamic analysis of coupled wind-train-bridge system considering tower shielding and triangular wind barriers", *Wind Struct.*, **21**(3), 311-329.
- Zhao, H., Zhai, W.M. and Chen, Z.G. (2015), "Effect of noise barrier on aerodynamic performance of high-speed train in crosswind", *Wind Struct.*, **20**(4), 509-525.

